Springer

KSME

Journal of Mechanical Science and Technology 31 (10) (2017) 5029~5039
www.springerlink.com/content/1738-494x(Print)/1976-3824(Online)
DOI 10.1007/s12206-017-0951-1

Optimization of a rectangular pin fin using elliptical perforations with different inclination angles †

Hisham H. Jasim[1,2,*] and Mehmet Sait Söylemez[2]

[1]*Department of Mechatronics Engineering, AL-Khwarizmi College of Engineering, Baghdad University, Iraq*
[2]*Department of Mechanical Engineering, Faculty of engineering, Gaziantep University, Turkey*

(Manuscript Received February 18, 2017; Revised May 7, 2017; Accepted June 3, 2017)

Abstract

An innovative form of a perforated fin (with inclination angles) was considered. In most previous studies, pin fins were perforated in a straight direction to improve the thermal performance of the heat sink. The present rectangular pin fin consisted of an elliptical perforation with two models and two cases. The signum function was used to model the opposite and mutable approach of the heat-transfer area. The degenerate hypergeometric equation was used as a new derivative method to determine a general solution and solved by Kummer's series. Two validation methods (previous work and Ansys 16.0 steady-state thermal analysis) were considered. The strong agreement of the validation results (0.31 %-0.52 %) showed the reliability of the presented model. The use of the perforated fin reduced the thermal resistance and improved the thermal performance of the pin fin by enhancing heat transfer and increasing the Nusselt number. Moreover, increasing the inclination angle, size, and number of perforations can optimize the present model by maximizing heat transfer and minimizing the weight and length of the pin fins. Increasing the open-area ratio minimizes entropy generation at a certain Rayleigh number and constant heat flux.

Keywords: Fin; Incline perforation; Natural convection; Degenerate hypergeometric equation; Optimization; Entropy minimization

1. Introduction

Developments in different applications, such as communication devices, mechatronics, and electronic devices, has resulted in increased heat transfer. Investigators use perforation toward a straight direction to improve the overall performance of heat sinks. Moreover, the shapes, sizes, numbers, and orientations of perforations are changed to optimize thermal performance.

Computational techniques are used by most investigators to solve governing equations. Five cases of an annular finned-tube system with a single perforation and three cases with multiple perforations were evaluated by Ref. [1] to determine which case exhibits the best performance in extreme climatic conditions. The single perforation location at 120° provided favorable results, and a 5.96 % enhancement in heat transfer was achieved. Circular, rectangular, and trapezoidal cross-section areas of a perforation were studied by Ref. [2] to determine the effects of the number and geometry of hollow fins on heat transfer by attaching rectangular fins to a microchannel heat sink. The results showed that improvement strongly depends on the number of hollow fins, and the influence of a hollow geometry is negligible. To demonstrate the advantages of perforation, Ref. [3] showed that a staggered thermal profile of perforated fins performs better than that of a solid elliptical pin fin in terms of static temperature, Nusselt number, and total heat calculated.

The effects of porosity on the performance of fins were investigated by Refs. [4, 5] for longitudinal and lateral perforation. A rectangular cross section with different dimensions and multiple perforations was considered to illustrate thermal enhancement in various operating conditions. High performances of perforated fins were observed, and effectiveness was increased by increasing the porosity ratio.

The Nusselt number and friction factor were optimized separately and together by Ref. [6] for the circular perforation of a rectangular cross section. The results showed that the high thermal performance of the pin fin depends on a low clearance ratio and a low inter-fin spacing ratio. Moreover, efficiency can be increased by 1.1 and 1.9 by using Reynolds numbers. Similarly, Refs. [7, 8] showed that the pin fin efficiency of a circular cross section can be increased by 1.4 and 1.6 by using circular perforation, with the Nusselt number being inversely proportional to the clearance and inter-fin spacing ratios. Ref. [9] showed that the thermal conductivity of a copper material

*Corresponding author. Tel.: +96 47901859706
E-mail address: ha19211@mail2.gantep.edu.tr, enghisham78@yahoo.com
† Recommended by Associate Editor Ji Hwan Jeong

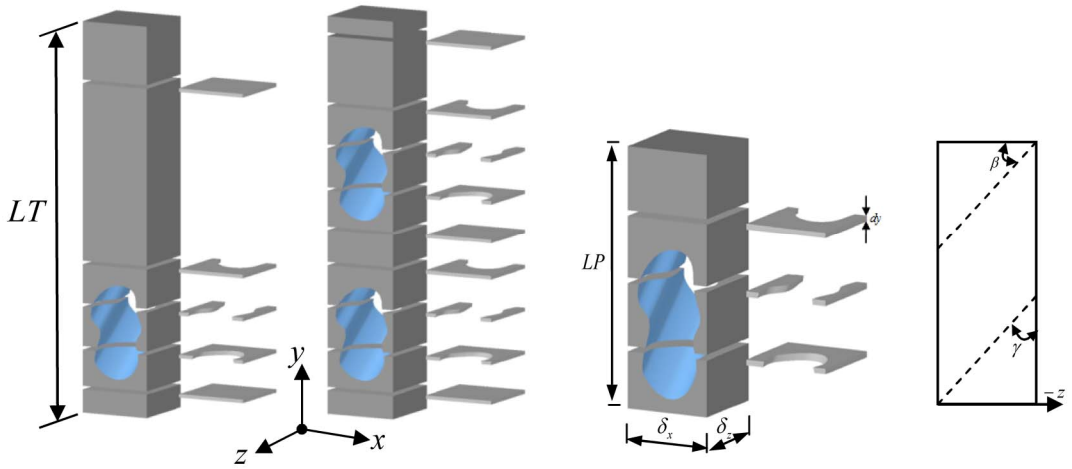

Fig. 1. Fin with inclined perforation: (a) Fin with one perforation; (b) fin with two perforations; (c) 3D model of the perforated region with different layers; (d) side view.

is higher than that of other materials, and a large number of perforated fins results in high heat transfer coefficients.

A large hollow pin diameter ratio provides a high augmentation factor for upward orientation, and the situation is reversed for sideward orientation for a circular pin fin using a circular perforation [10].

The Reynolds number and perforation size significantly influence the Nusselt number for rectangular fins using lateral perforations (square and circular) [11]. A perforated pin fin in a cylindrical channel was tested by Ref. [12] by changing the number of circular perforations. The number of perforations significantly increases convective heat transfer by about 30 % to 40 %.

An analytical study [13] revealed that the temperature distribution of a perforated fin reaches the temperature distribution equation of a perforated flat plate by using a mathematical model solved by Fourier series and Flocke's theory. Ref. [14] reported a decrease in the thermal conduction resistance of a pin fin due to triangular perforation, and this decrease leads to improved heat dissipation calculated by a variation approach and finite element techniques. Ref. [15] applied the same technique to determine the effects of the orientations of rectangular perforations under natural convection. The inclined orientation is suitable for small thickness and low thermal conductivity, whereas the parallel orientation is suitable for large thickness. Ref. [16] concluded that increasing perforation size and thermal conductivity leads to augmentation of heat transfer from a rectangular fin.

In Ref. [17], thermal resistance was optimized in pin-fin heat sinks with a constant Reynolds number. Increased number of fins leads to a decrease in thermal resistance without a limit for a height of 40 mm. The optimum number of fins can be achieved at heights of 20 and 30 mm. Furthermore, entropy generation was calculated as another means of optimization. The results showed that the highest entropy generation is associated with the highest Reynolds number, and entropy generation decreases with the increase in the open area ratio.

Ref. [18] used momentum and energy equations to calculate the entropy generation for rectangular cavities under natural convection at five aspect ratios and five Rayleigh numbers. Entropy generation increases linearly with the aspect ratio and Rayleigh number. Entropy generation is also increased by the Rayleigh number at a certain aspect ratio. Ref. [19] investigated the effects of the channel aspect ratio, fin spacing ratio, and heat sink material on the entropy generation rate of a microchannel heat sink. Increments in the volume flow rate lead to increments in the optimum channel aspect and fin spacing, resulting in a decrease in thermal resistance.

All recent studies used straight perforations with different shapes, sizes, and orientations to improve the overall performance of rectangular plates, pins, and annular fins.

The approach introduced in the current work presents two novel points. First, inclined perforation was considered in the geometric model. Second, in the analytical process, a new differential technique was used to derive the general form of temperature distribution regardless of the perforation shape. Moreover, the signum function was used to model the opposite and mutable approach of the heat transfer area. A mathematical model was utilized to study the thermal behavior of the present model, and entropy generation minimization was adopted as an optimization method.

2. Geometric model

The inclined perforated region of the pin fin is shown in Fig. 1. An undefined section of perforation was considered in a general form. Inclination began from $\beta = 0$ in the straight perforation. The fin possessed a rectangular cross-section area with one and two perforations. The base fin is located on the *x*-*z* plane and *y*-axis at the fin length. Given the inclined perforation, the heat transfer area changes with the *y*-direction and with a change in the inclination angle.

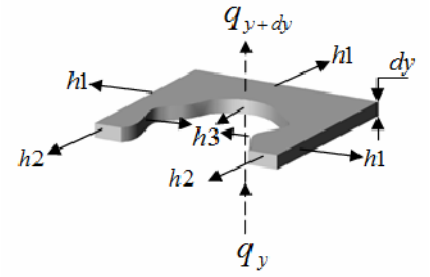

Fig. 2. Element description.

3. Energy analysis and assumption

Energy balance was applied to the element shown in Fig. 2 to obtain the differential equation of energy [Eq. (1)] in the perforated region.

The heat transfer analysis conducted in this study relied on of the following assumptions.

1. Steady heat conduction with no heat generation.
2. 1D heat transfer analysis depends on the impairment of the Biot number at *z*- and *x*-axes.
3. Constant conductivity ($k = 222\ W/m.K$).
4. Constant base temperature.
5. Insulation of the tip fin, and radiation effects are neglected.
6. Uniform ambient temperature and uniform convection heat transfer coefficient.
7. Convection coefficient is divided into three types [external non-perforated (h1), external perforated (h2), and internal perforated (h3)].

$$\frac{d}{dy}(A_{cond.}\frac{d\theta}{dy})dy=[h1P_{conv1}+h2P_{conv2}+h3P_{conv3}]\frac{\theta\,dy}{k} \qquad (1)$$
$$\theta=T(y)-T_{air}$$

where A_{cond} is the conduction area and P_{conv} is the perimeter of the convection. Various convection heat transfer coefficients appeared due to the inclined perforation. Moreover, the convection coefficients depended on the properties of the cooling fluid, specifications of the perforated fin, and the open perforated ratio (R_{OP}). R_{OP} represents the ratio of the actual perforated area to the maximum perforation effects.

Empirical correlations for the Nusselt number (Nu) obtained from Refs. [20, 21] were used to determine convection coefficients h_1 and h_2, respectively. The correlation from Ref. [22] was modified for use in the calculation of h_3, as described in Ref. [23]. Furthermore, the temperature distribution of the solid regions was calculated according to Ref. [20].

4. General solution

Eq. (1) can be represented by using the Degenerate hypergeometric equation (DHE) [23, 24].

$$\vartheta\frac{d^2u}{d\vartheta^2}+(ku1-\vartheta)\frac{du}{d\vartheta}-(ku2)u=0 \qquad (2)$$

where $u=e^{\vartheta/2}G$, $\vartheta=\xi^2\sqrt{p1}$, $\theta=G/\sqrt{A_{cond.}}$

$\xi=y+\dfrac{p2}{2p1}$, $ku1, ku2=$ constants.

The DHE equation was solved by Kummer's series [25, 26] to obtain the general solution of the present model.

$$u(\vartheta)=CO_i\,\varphi(ku1,ku2,\vartheta)+CO_{i+1}\psi(ku1,ku2,\vartheta),\quad i=1,3,5,.... \qquad (3)$$

where

φ = Confluent hypergeometric function of the first type,

ψ = Confluent hypergeometric function of the second type,

CO = Constant for the general solution.

The boundary conditions for the constant base temperature are

$$u\Big|_{\vartheta=-\frac{p2^2}{4p1^{3/2}}}=\theta_b\sqrt{A_b}\,e^{\frac{p2^2}{8p1^{3/2}}}\quad,\quad \frac{du}{d\vartheta}\Big|_{\vartheta=(LP+\frac{p2}{2p1})^2\sqrt{p1}}=0$$

which are compatible with the boundary conditions in the original form.

$$\theta\big|_{y=0}=\theta_b\quad,\quad \frac{d\theta}{dy}\Big|_{y=LP}=0\,.$$

The solution of Eq. (3) with the abovementioned boundary conditions leads to the temperature distribution equation.

$$\frac{\theta(y)}{\theta_b}=\frac{e^{\frac{-(y+\frac{p2}{2p1})^2\sqrt{p1}}{2}}}{\sqrt{A_{cond.}}}\,[\zeta10\ \varphi(ku1,ku2,((y+\frac{p2}{2p1})^2\sqrt{p1})) \qquad (4)$$
$$-\zeta11\ \psi(ku1,ku2,((y+\frac{p2}{2p1})^2\sqrt{p1}))]$$

Where: P1, P2 constants [23]

$$\zeta10=\frac{\zeta4\zeta6+\zeta8\zeta9}{\zeta1\zeta2(\zeta4\zeta6+\zeta8\zeta9)-\zeta1\zeta3(\zeta4\zeta5+\zeta7\zeta9)}$$

$$\zeta11=\frac{\zeta4\zeta5+\zeta7\zeta9}{\zeta4\zeta6+\zeta8\zeta9}\zeta10\ ,\quad \zeta1=\frac{e^{-\frac{p2^2}{8p1^{3/2}}}}{\sqrt{A_b}}$$

$$\zeta2=\varphi(ku1,ku2;\frac{p2^2}{8p1^{3/2}})\ ,\quad \zeta3=\psi(ku1,ku2;\frac{p2^2}{8p1^{3/2}})$$

$$\zeta4=\frac{e^{\frac{-(LP+\frac{p2}{2p1})^2\sqrt{P1}}{2}}}{\sqrt{A_{cond.})_{LP}}}\ ,\ \zeta5=\varphi'[ku1,ku2;((LP+\frac{p2}{2p1})^2\sqrt{p1})]$$

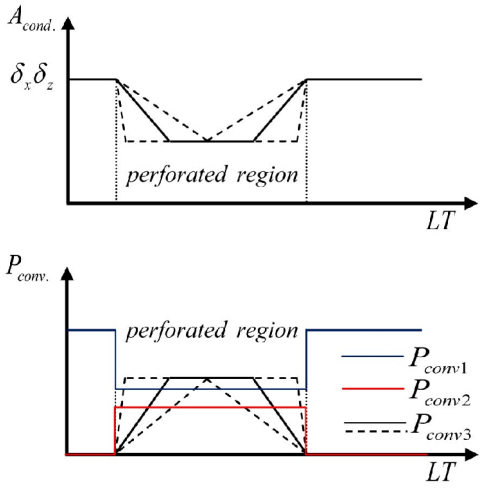

Fig. 3. Change in the heat transfer area (Conduction area and convection perimeter).

$$\zeta 6 = \psi'[ku1, ku2; ((LP + \frac{p2}{2p1})^2 \sqrt{p1})]$$

$$\zeta 7 = \varphi(ku1, ku2; ((LP + \frac{p2}{2p1})^2 \sqrt{p1}))$$

$$\zeta 8 = \psi(ku1, ku2; ((LP + \frac{p2}{2p1})^2 \sqrt{p1}))$$

$$\zeta 9 = -\frac{(LP + \frac{p2}{2p1})(\sqrt{p1}\sqrt{A_{cond})_{LP}})\, e^{\frac{-(LP+\frac{p2}{2p1})^2\sqrt{P1}}{2}}}{A_{cond})_{LP}} - \frac{\frac{A'_{cond.})_{LP}\, e^{\frac{-(LP+\frac{p2}{2p1})^2\sqrt{P1}}{2}}}{2\sqrt{A_{cond})_{LP}}}}{A_{cond})_{LP}}.$$

5. Modeling of the heat transfer area

A change in the heat transfer area, conduction area $A_{cond.}$, and convection perimeter $P_{conv.}$ depends on the y-axis and inclination angle and leads to many difficulties when calculating the area at any specification. The extreme ends for $A_{cond.}$ and $P_{conv.}$ can be represented by a point or a line depending on the inclination angle and size of the perforation, as shown in Fig. 3.

The signum function (sgn) [27] was used to represent the opposite and mutable approach of variables $A_{cond.}$ and $P_{conv.}$. Figs. 4 and 5 show the change in the perforated section with the y-axis based on the inclination angle. The equations of heat transfer area were derived and formulated based on a group of constants (a, a_1, a_2), as shown in Table 1. Moreover, Eqs. (5)-(8) were used to calculate the heat transfer area at any specification.

$$A_{cond.} = \frac{AA}{a}(a_1 - y)\,\mathrm{sgn}(a - y) + (\delta_z\, \delta_x) - AA \tag{5}$$

Table 1. Constant value.

Region no.	Constant value	
	a_1	a_2
1	a	δ_x
2	y	0
3	LP-a	δ_x

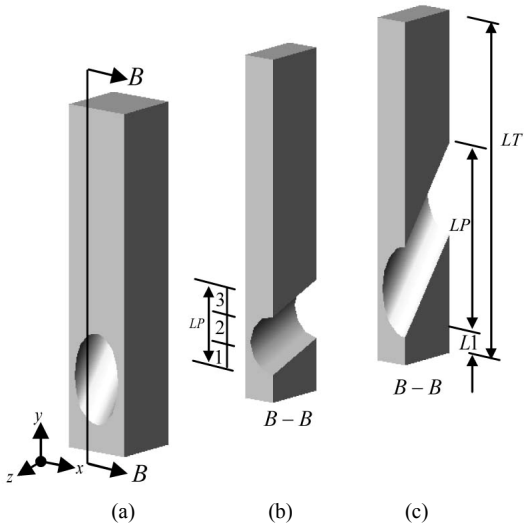

Fig. 4. Ellipse perforated at different angles: (a) 3D plot; (b) small angle; (c) large angle.

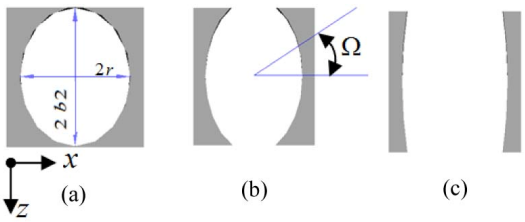

Fig. 5. Ellipse perforated section at (a) large angle; (b) smaller than a; (c) smaller than b.

$$P_{conv1} = 2\delta_z + a_2 \tag{6}$$

$$P_{conv2}\, dy = \int_{-b3}^{b3} (\delta_x - 2r\sqrt{1 - \frac{y^2}{b3^2}})\, dy \tag{7}$$

$$P_{conv3} = 4\int_0^{w1} \sqrt{(r^2 \cos^2\Omega) + (b2^2 \sin^2\Omega)}\; d\Omega \tag{8}$$

where

$$\mathrm{sgn}(a - y) = \tanh[(N(a - y)], \quad N >> 1$$

$$zp = z + \frac{\delta_z}{2}\ , w1 = \tan^{-1}\frac{\delta_z/2}{r\sqrt{1 - \frac{(\delta_z/2)^2}{b2^2}}}\ , a = \delta_z \tan\beta$$

Table 2. Grid-independent studies.

Inclination angle		Grid	Min. temperature
Case-1-	β = 8	115901	87.1
		137423	87.69
		148908	87.939
		158390	87.945
	β = 22	129236	86.882
		147208	87.121
		160411	87.649
		172179	87.66

Table 3. Grid-independent studies.

Inclination angle		Grid	Min. temperature
Case-2-	β = 9	119932	85.86
		142111	86.24
		160854	86.528
		171546	86.53
	β = 25	190234	85.29
		211906	85.78
		219523	86.16
		231248	86.18

$$AA = (\pi\, r\, b2) - 4r \int_{-b2}^{-\delta_z/2} \sqrt{1 - \frac{zp^2}{b2^2}}\; dzp\,,$$

$$b2 = \frac{1}{2}(\delta_z + \frac{2r - \delta_z \sin\beta}{\cos\beta}\tan\gamma)\,, \quad b3 = r/\cos\beta\,.$$

The results of the two models (I and II) were calculated for natural convection heat transfer and Rayleigh number (Ra = 10^6) by using Matlab language (R2014a). Models I and II are described as follows:

Model-I- $\delta_x = \delta_z = 0.01\,(m),\ r = 0.0035(m), LT = 0.05(m)$

Model-II- $\delta_x = \delta_z = 0.01\,(m), r = 0.004(m), LT = 0.05(m)$.

6. Numerical solutions and simulation

Thermal analysis was conducted using Ansys 16.0 steady-state thermal analysis for models I and II. Several grids were studied to ensure that the solutions are independent grids, as shown in Tables 2 and 3. A highly accurate grid is required for the perforated region due to curvatures and edges. This problem is solved by changing the advanced size function to become proximity and curvatures. Face size was calculated according to Eq. (9).

$$\text{Max. face size} = \frac{\delta_x \text{ or } \delta_z}{NG},\ NG = 20 - 30\,. \tag{9}$$

The minimum temperature was compared until independent grids were successfully obtained. All results were calculated at

(a) (b)

Fig. 6. Grid configuration for case -1-: (a) $\beta = 8$; (b) $\beta = 22$.

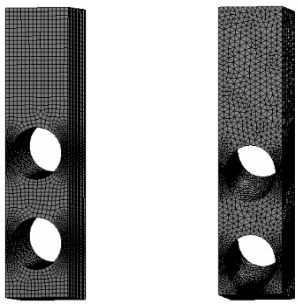

(a) (b)

Fig. 7. Grid configuration for case -2-: (a) $\beta = 9$; (b) $\beta = 25$.

the base temperature (90 °C) and air temperature (25 °C). Two cases (-1- and -2-) were adopted to show the grid configurations, as shown in Figs. 6 and 7. The descriptions of the two cases are as follows:

Case -1- is model I with one perforation, and case -2- is model II with two perforations.

7. Results and discussion

7.1 Validation of the analytical model

Two validation methods were considered. In Ref. [13], the Kirpikov formula was used in the first method to validate straight perforation. Kirpikov reported that the temperature distribution along the perforated fin is a function of the Biot number. The equation to calculate the Biot number (Bi) of the present model is

$$Bi = \frac{LT^2[\sum h_i\, A_{convi}]}{k \int A_{cond}\, dy} \qquad i = 1, 2, 3\,. \tag{10}$$

The high similarity between the results is evident below the perforation region, but the difference between the results increases in the perforation region. The maximum difference reached 0.52 %, as shown in Fig. 8. The difference in the results decreased above the perforation region.

The reasons for the difference in the results can be explained as follows:

(1) In the Kirpikov model, the heat transfer coefficient was

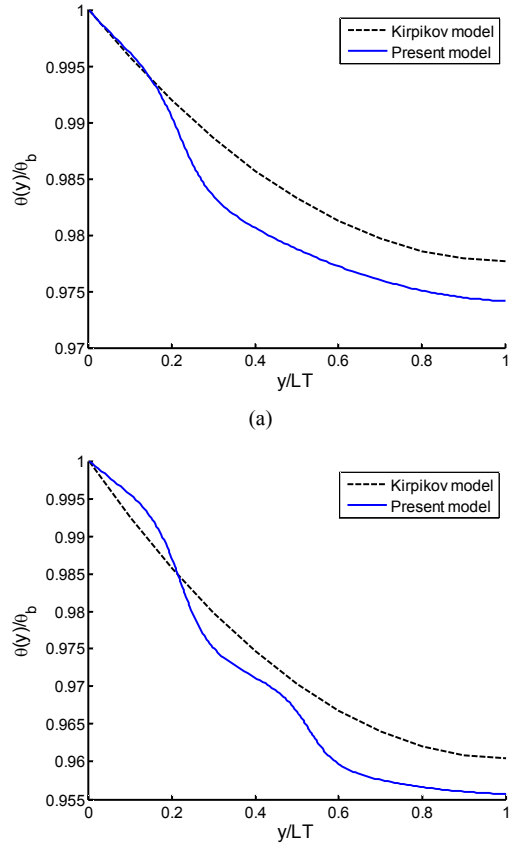

Fig. 8. Comparisons of the present model and the Kirpikov model for rectangular perforation and $\beta = 0^{\circ}$: (a) Case -1-; (b) case -2-.

not classified into three regions.

(2) In the Kirpikov model, an approximate solution (Fourier series) was adopted.

(3) In the Kirpikov model, the convection coefficient of the inner surface was assumed to be a ratio from the external coefficient (independent of the size and length of the perforation).

The temperature difference decreased with the inclination angle. An additional temperature decrease can occur with an increase in the size and number of perforations. This phenomenon is due to increase in the Biot number as a result of the decrease in thermal resistance.

In the second validation method, two inclination angles were adopted for each case considered in the calculation process. The distribution of fin temperature (θ/θ_b) was calculated along the fin length (y/LT) to demonstrate the convergence between the analytical solution (using the present mathematical techniques) and numerical solution (using Ansys simulation), as shown in Figs. 9 and 10. An increase in the inclination angle led to a reduced fin temperature as a result of the following reasons.

- Increase in the inner convection area.
- Distribution of the inner convection area in the large length on the *y*-axis.

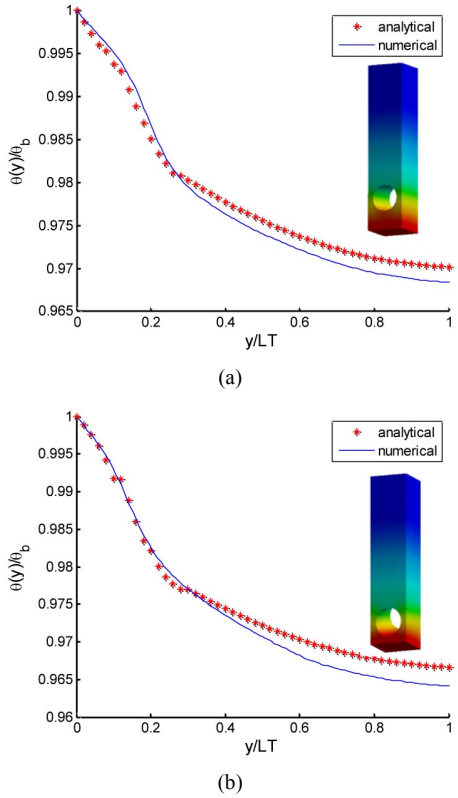

Fig. 9. Comparison of analytical and numerical results for case -1-: (a) $\beta = 8^{\circ}$; (b) $\beta = 22^{\circ}$.

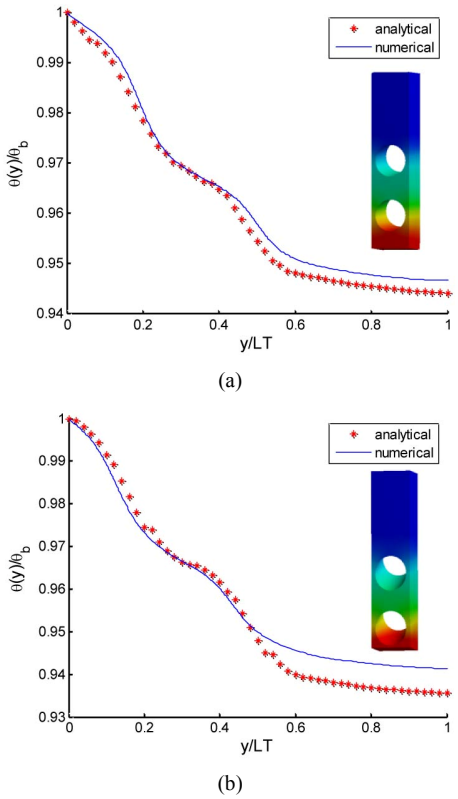

Fig. 10. Comparison of analytical and numerical results for case -2-: (a) $\beta = 9^{\circ}$; (b) $\beta = 25^{\circ}$.

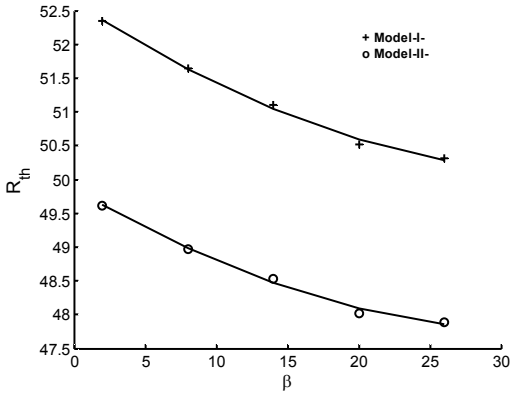

Fig. 11. Variation in R_{th} with inclination angle.

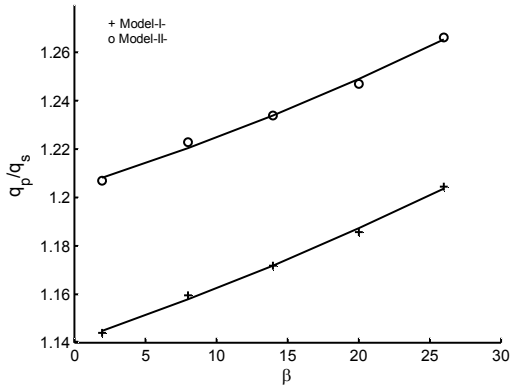

Fig. 13. Effects of inclination angle on heat transfer ratio.

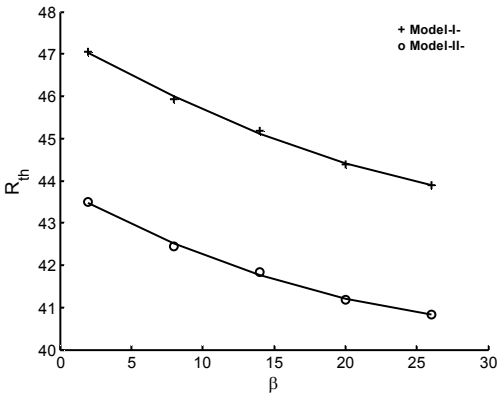

Fig. 12. Variation in R_{th} with inclination angle.

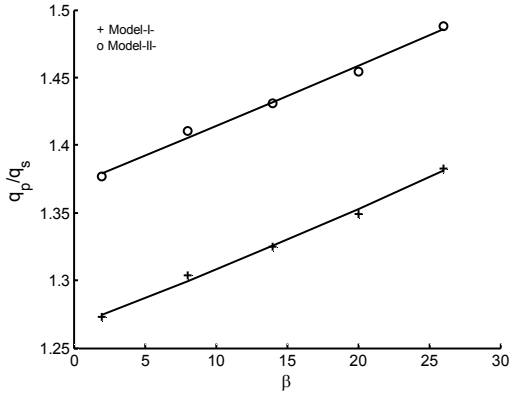

Fig. 14. Effects of inclination angle on heat transfer ratio.

• Increase in the external perforated area.

Additionally, increased perforation size and number can lead to additional improvements in the convection area.

The profile of the results is similar for both analytical and numerical models. The results also show a resemblance below the fin length of 0.2 or 0.3 based on the inclination angle. Above these limits, the maximum difference can reach 0.31 %.

7.2 Effects of inclination on thermal resistance

The heat transfer area was changed due to the inclined perforation, leading to variable thermal resistance (R_{th}) along the fin length. According to the insulated fin tip, the equation to calculate the thermal resistance is described as

$$R_{th} = \frac{A_{conv}}{\int \sqrt{h\,p\,k\,A}\,dA_{conv}\,\tanh\left(\frac{\int \sqrt{h\,p/kA}\,dA_{conv}}{A_{conv}} LT\right)} \tag{11}$$

where

$$A_{conv.} = \int_0^{LT} (P_{conv1} + P_{conv2} + P_{conv3})\,dy\,.$$

In the inclined perforation region, the conduction area was replaced by the convection area, leading to improved thermal resistance. Figs. 11 and 12 show the change in thermal resistance with inclination angles for one and two perforations, respectively. All results show decrements in thermal resistance with an increase for both inclination angle and perforation size. An increase in the number of the perforations also leads to improvement of thermal resistance.

7.3 Effects of inclination on heat ratio

An increase in heat transfer is possible according to the multiple advantages obtained from the inclined perforation and decrements in temperature distributions along the fin. The heat transfer ratio, q_p / q_s, is the ratio between the heat transfer of a perforated fin to the heat transfer of a solid fin at the same properties.

$$q_{p\ or\ s} = -k\ A_b \left.\frac{d\theta}{dy}\right|_{y=0}\,. \tag{12}$$

An increase in temperature slopes with the inclination angle leads to an improved heat transfer ratio by approximately 1.14-1.26 times depending on the size of the one perforation,

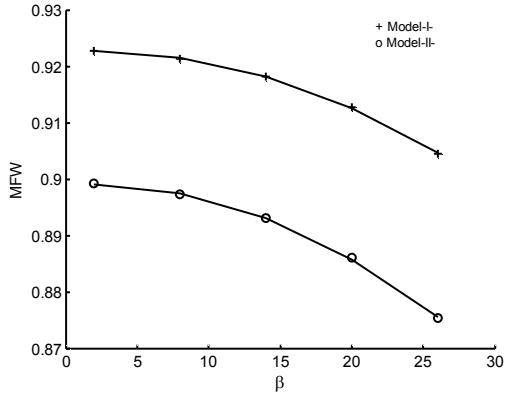

Fig. 15. Minimization of fin weight with inclination angle.

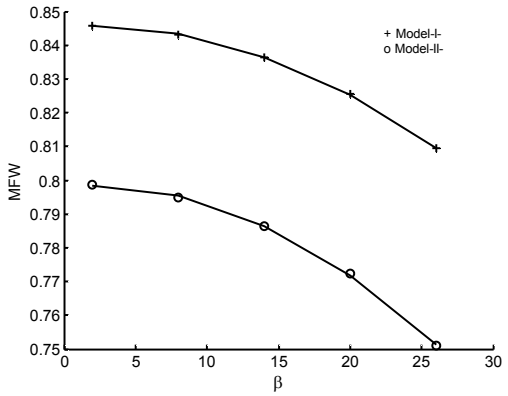

Fig. 16. Minimization of fin weight with inclination angle.

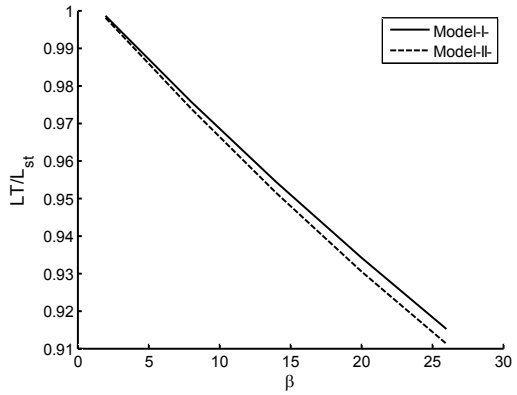

Fig. 17. Variation in length ratio with inclination angle.

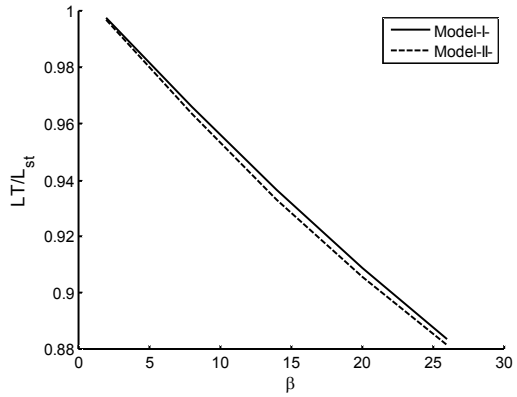

Fig. 18. Variation in the length ratio with inclination angle.

as shown in Fig. 13. Further improvements in the heat ratio (approximately 1.25-1.48) may occur when two perforations are used, as shown in Fig. 14.

8. Optimization

One of the goals of this work was to determine a new pin fin geometry that would minimize fin length and fin weight while maximizing heat transfer. Optimization was performed on a pin fin with perforations of various numbers, sizes, and inclination angles, with the Rayleigh number and base temperature as constants.

8.1 Minimizing the fin weight

Minimization of the expenditure of the fin material can be achieved by using perforation. This advantage can be increased when using an inclined perforation as a result of reduced conduction area, as shown in Figs 15 and 16.

Minimization of fin weight (MFW) was achieved with an increase in the inclination angle, size, and number of perforation because all these parameters lead to an increase in the convection surface area by reducing the conduction heat transfer area.

$$MFW = \frac{W_s - W_p}{W_s} \tag{13}$$

where W_s = weight of the solid fin and W_p = weight of the perforated fin.

8.2 Minimizing fin length

In this step, the amount of heat transfer and fin dimensions for straight perforation were regarded in the main design. Fin length was calculated according to Eq. (11). The length ratio (LT/L_{st}) between the model length and fin length of the straight perforation was calculated. Figs. 17 and 18 show the variations in the length ratio for single and double perforations, respectively. The length ratio decreased with an increase in inclination angle. The length ratio was also sensitive to inclination angle, whereas it changed smoothly with the change in perforation size. In addition, increments in perforation number led to an improvement in the length ratio.

where L_{st} is the fin length required to transfer heat with straight perforation.

The capability of the fin to transfer heat increased with inclination angle as a result of decreasing the thermal resistance. This phenomenon led to the minimization of the fin length

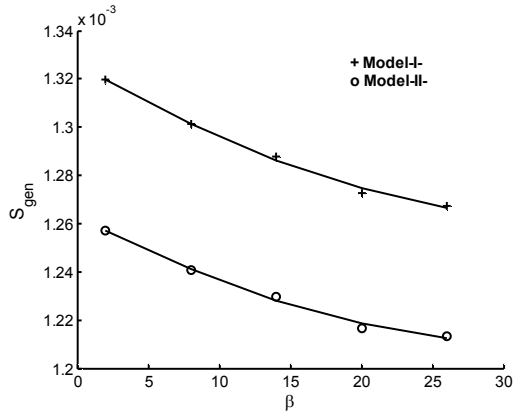

Fig. 19. Variation in S_{gen} with inclination angle.

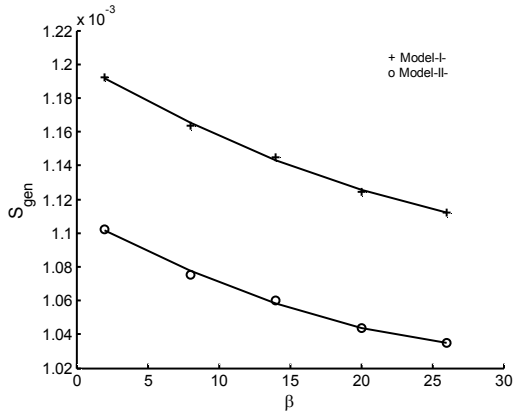

Fig. 20. Variation in S_{gen} with inclination angle.

required to transfer the same amount of heat by increasing the inclination angle, size, and number of perforations.

9. Entropy generation minimization

The goal of this step was to minimize the entropy generation ($S_{gen.}$) related to the inclined perforation in various conditions. To show the effects of inclination angle on entropy generation, constant heat flux at the base fin was considered. For the steady state, the second law of thermodynamics can be written as [28, 29]

$$S_{gen} = m^{\bullet} \Delta S - \iint_A \frac{q_{conv}\, dA}{T(y)} . \tag{14}$$

According to the concept of enthalpy change, entropy generation can be calculated with Eq. (15).

$$S_{gen} = \iint_A \frac{q_{conv}\,(T(y) - T_{air})dA}{T(y)T_{air}} - \frac{m^{\bullet}\Delta P}{\rho T_{air}} . \tag{15}$$

As shown in the equation, entropy generation is a function of thermal resistance and pressure drop. For low-velocity conditions, the second term can be neglected [28, 30].

Figs. 19 and 20 show the decrements in entropy generation with the increase in inclination angle and perforation size. Increasing the number of perforations led to an improvement in the entropy generation value.

10. Conclusion

This study proposed the use of inclined perforations as a new approach to improve the performance of pin fins. In the solution process, two novel methods were presented: *Modeling of the opposite approach of the variable heat transfer area based on the signum function* and *solving the energy differential equation using* DHE. An elliptical cross-section area of the perforation with multiple sizes, numbers, and angles was considered to verify the accuracy and flexibility of the mathematic model. The high level of agreement of the validation results revealed the high reliability of the present mathematical model. Consequently, the general solution of the present study can be regarded as a basis to resolve any perforation shape by modeling the heat transfer area.

Increasing the inclination angle, perforation size, and number of perforations led to a decrease in the temperature of the fin for the following reasons:

- Increase in the inner convection area.
- Distribution of the inner convection area on the large length on the *y*-axis.
- Increase in the external perforated area.
- The conduction area replaced by the convection area was increased.

These advantages led to decreased thermal resistance and improved thermal performance of the pin fin by enhancing the heat transfer. An increase in the parameters (inclination angle, size, and number of perforations) can be used to optimize the present model by minimizing the weight and length of the pin fin.

Entropy generation was minimized with an increase in inclination angle and perforation size for constant heat flux as a result of the decrease in thermal resistance. Further decrements in entropy generation can occur if the number of perforations was increased. However, the optimum point did not appear within the range of the inclined angle adopted in this study.

Nomenclature

h	: Convection coefficient (W/m^2. °C)
LP	: Length of the perforated region on *y*-axis (m)
LT	: Total fin length (m)
$m^{\bullet}$	: Mass flow rate (kg/s)
q	: Heat transfer (W)
S	: Entropy (W/ K)
T	: Temperature (°C)

Subscript

gen	: Generation
p	: Perforated
s	: Solid
st	: Straight perforated

Greek letters

β,γ	: Inclination angles (degrees)

References

[1] R. K. Banerjee and M. Karve, Evaluation of enhanced heat transfer within a four row finned tube array of an air cooled steam condenser, *Numerical Heat Transfer, Part A*, 61 (2012) 735-753.

[2] H. J. Tony Tan, M. Z. Abdullah and M. Abdul Mujeebu, Effects of geometry and number of hollow on the performance of rectangular fins in microchannel heat sinks, *J. of Thermal Science and Technology - TIBTD Printed in Turkey* (2013).

[3] M. Baruah, A. Dewan and P. Mahanta, Performance of elliptical pin fin heat exchanger with three elliptical perforations, *CFD Letters*, 3 (2) (2011) [S2180-1363(11)3265-X].

[4] M. R. Shaeri and M. Yaghoubi, Thermal enhancement from heat sinks by using perforated fins, *Energy Conversion and Management,* 50 (2009).

[5] M. R. Shaeri, M. Yaghoubi and K. Jafarpur, Heat transfer analysis of lateral perforated fin heat sinks, *Applied Energy*, 86 (2009).

[6] B. Sahin and A. Demir, Performance analysis of a heat exchanger having perforated square fins, *Applied Thermal Engineering,* 28 (2008) 621-632.

[7] B. Sahin and A. Demir, Thermal performance analysis and optimum design parameters of heat exchanger having perforated pin fins, *Energy Conversion and Management*, 49 (2008) 1684-1695.

[8] A. B. Dhumne and H. S. Farkade, Heat transfer analysis of cylindrical perforated fins in staggered arrangement, *International Journal of Innovative Technology and Exploring Engineering (IJITEE)*, 2 (5) (2013) April.

[9] S. D. Bahadure and G. D. Gosavi, Enhancement of natural convection heat transfer from perforated fin, *International Journal of Engineering Research*, 3 (9) (2014) 531-535.

[10] E. A. M. Elshafei, Natural convection heat transfer from a heat sink with hollow / perforated circular pin fins, *Energy*, 35 (2010) 2870e2877.

[11] K. H. Dhanawade, V. K. Sunnapwar and H. S. Dhanawade, Thermal analysis of square and circular perforated fin arrays by forced convection, *International Journal of Current Engineering and Technology* (2014).

[12] A. Fule, A. M. Salwe, A. Z. Sheikh and N. Wasnik, Convective heat transfer comparison between solid and perforated pin fin, *International Journal of Mechanical and Robotics Research*, 3 (2) (2014) April.

[13] V. A. Kirpikov and I. I. Leifman, Calculation of the temperature profile of a perforated fin, instituted of chemical apparatus design, *Moscow*, 23 (2) (1972) 316-321, August.

[14] A. H. M. AlEssa, One-dimensional finite element heat transfer solution of a fin with triangular perforations of bases parallel and towered its base, *Arch. Appl. Mech.,* 79 (2009) 741-751.

[15] A. H. Al-Essa and F. M. S. Al-Hussien, The effect of orientation of square perforations on the heat transfer enhancement from a fin subjected to natural convection, *Heat and Mass Transfer*, 40 (2004) 509-515.

[16] D. G. Kumbhar, N. K. Sane and S. T. Chavan, Finite element analysis and experimental study of convective heat transfer augmentation from horizontal rectangular fin by triangular perforations, *International Conference on Advances In Mechanical Engineering, National Institute of Technology*, Surat - 395 007, Gujarat, India (2009) August, 376-380.

[17] M. L. Elsayed and O. Mesalhy, *Studying the performance of solid/perforated pin-fin heat sinks using entropy generation minimization*, Springer-Heat Mass Transfer (2014).

[18] R. De C. Oliveski, M. H. Macagnan and J. B. Copetti, Entropy generation and natural convection in rectangular cavities, *Applied Thermal Engineering*, 29 (2009) 1417-1425.

[19] W. A. Khan, J. R. Culham and M. M. Yovanovich, Optimization of microchannel heat sinks using entropy generation minimization method, *IEEE Transactions on Components and Packaging Technologies*, 32 (2) (2009).

[20] Incropera, Dewitt, Bergman and Lavine, *Fundamental of heat and mass transfer*, 6th Ed., John Wiley & Sons (2007) 95-160 and 560-594.

[21] Z. Wu, W. Li, Z.-J. Sun and R.-H. Hong, Modeling natural convection heat transfer from perforated plates, *Journal of Zhejiang University-Science A*, 13 (5) (2012) 353-360.

[22] G. D. Raithby and K. G. T. Hollands, Natural convection, W. M. Rohsenow, J. R. Hartnett, Y. I. Cho, *Handbook of heat transfer*, 3rd edition, MCGRAW-HILL (1998) 4-1 to 4-80.

[23] H. H. Jasim and M. S. Söylemez, The temperature profile for the innovative design of the perforated fin, *Int. Journal of Renewable Energy Development*, 5 (3) (2016) 259-266.

[24] H. H. Jasim and M. S. Söylemez, Enhancement of natural convection heat transfer of pin fin having perforated with inclination angle, *J. of Thermal Science and Technology*, Isı Bilimi ve Tekniği Dergisi, 36 (2) (2016) 111-118.

[25] A. D. Polyanin and V. F. Zaitsev, *Hand book of exact solution for ordinary differential equations*, 2nd Ed. (USA), By Chapman & Hall/Crc (2003) 213-490.

[26] M. Hazewinkel, *Encyclopaedia of mathematics: A-integral —coordinates*, Springer Science and Business Media (1995) 105-110 and 797-800.

[27] J. W. Harris and H. Stocker, *Hand book of mathematics and computational science*, Springer (USA) (1998) 130-150.

[28] C. W. de Silva, *Mechatronic systems devices*, Design, Control, Operation, Taylor & Francis Group (2008).
[29] S. A. E. S. Ahmed, O. M. Mesalhy and M. A. Abdelatief, Heat transfer characteristics and entropy generation for wing-shaped-tubes with longitudinal external fins in cross-flow, *Journal of Mechanical Science and Technology*, 30 (6) (2016) 2849-2863.
[30] C. W. de Silva, *Mechatronics an integrated approach*, Taylor & Francis Group (2005).

Hisham H. Jasim is the Lecturer in the Department of Mechatronics, Al-Khawarizmi College of Engineering, University of Baghdad. His research interests are in the areas of heat transfer applications, the simulation and experiments in heat sink design, developments in the design of thermal systems, heat source in electronic Packages and advanced conduction problems.